*Journal of the Nigerian Association of Mathematical Physics*
*Volume 31,* **(July,** *2015***), pp 71 – 78**


# The Effect of Sputtering Parameters on the Hardness and Fracture Toughness of Copper Oxide Thin Films Prepared by Reactive Magnetron Sputtering

***T.H. Darma***

**Department of Physics, Bayero University, Kano, P.M.B. 3011, Kano-Nigeria.**

## *Abstract*

***The effects of deposition parameters on some mechanical properties of copper oxide thin films are investigated. A Hysitron Tribo-Nanomechanical system and a Shimadzu Micro Hardness tester with a diamond Vickers indenter were used to perform Nanoindentations and Micro indentations at various loads on copper oxide thin films prepared on glass slides at various deposition conditions. The films are found to be predominantly of the cuprous oxide ($Cu_2O$) phase. The mechanical properties evaluated comprises of hardness found to be in the range of 4.13 – 4.99 GPa, elastic modulus of 52.24 – 66.69 GPa, plasticity index of 0.061 – 0.079, and fracture toughness of 0.64 ± 0.26 - 1.55 ± 0.49 MPa.$m^{½}$. The findings are indications that copper oxide thin films exhibit fracture brittle in nature.***

**Keywords:** Reactive magnetron sputtering, copper oxide, fracture toughness.

## 1.0 Introduction

Indentation is one of the most commonly applied means of measuring the mechanical properties of materials. In a traditional indentation test (macro or micro indentation), a hard tip whose mechanical properties are known (frequently made of a very hard material like diamond) is pressed into a sample whose properties are unknown. The hardness of a sample can be determined by three methods namely scratching, static indentation, and rebound or dynamic hardness test. During indentation, the load placed on the indenter tip is increased as the tip penetrates further into the specimen and soon reaches a user-defined value. At this point, the load may be held constant for a period or removed.

Nanoindentation improves on macro and micro indentation tests by indenting on the nanoscale with a very precise tip shape. This enables the determination of the hardness of the thin film by penetrating the coating and not the substrate. The indent impression on the coating is so small to be measured optically, and thus requires a method that will monitor the load and penetration depth and provide real-time load-displacement data while the indentation is in progress. A typical example is the Hysitron Tribo-Scope Nanomechanical testing system.

In nanoindentation small loads and tip sizes are used, so the indentation area may only be a few square micrometers or even nanometers. As a result, an indenter with a geometry known to high precision (usually a Berkovich tip, which has three-sided pyramid geometry) is employed. During the course of the instrumented indentation process, a record of the depth of penetration is made, and then the area of the indent is determined using the known geometry of the indentation tip. In the process, various parameters, such as load and depth of penetration, can be measured. A record of these values is plotted to create a load-displacement curve. The depth-sensing indentation technique uses the fitted load-depth penetration curve in order to obtain the hardness H and the reduced elastic modulus $E_r$ of a coating. A cross-section of the indentation with essential parameters to determine hardness H and reduced modulus is shown in Fig. 1.

Corresponding author: T.H. Darma, E-mail: thdarma.phy@buk.edu.ng, Tel.: +2348107596053

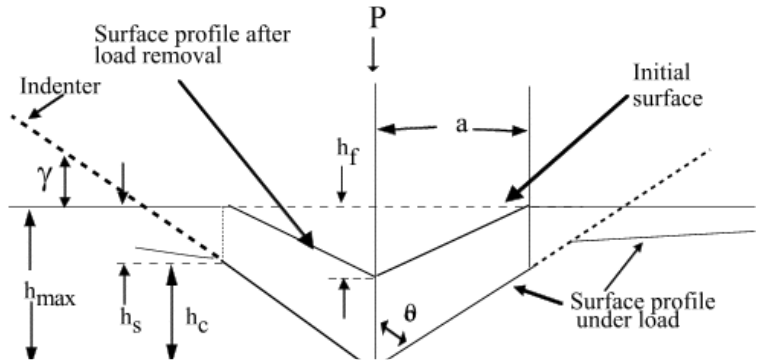


**Fig. 1:** Cross-section of an indentation with essential parameters to determine hardness H and reduced modulus $E_r$ [1]

The parameter $S_{max}$ is the maximum stiffness or the linear slope S = dp/dh of the first third of the load-penetration curve which belongs to the elastic relaxation, $P_{max}$ is the maximum load, $h_{max}$ the maximum depth, $h_c$ is the contact depth, $h_f$ the residual depth of indentation, and $h_p$ the intercept depth.
The area of the residual indentation in the sample is measured and the hardness, *H*, is defined as the maximum load, $P_{max}$, divided by the residual indentation area, $A_c$, or

$$H = \frac{Pmax}{A_c} \quad \text{.....} \qquad (1)$$

The reduced modulus was calculated using Equation (2).

$$E_r = \frac{\sqrt{\pi}}{2\sqrt{A(h_c)}} S \quad \text{…….....} \qquad (2)$$

where S is the contact stiffness.
The elastic modulus of the specimen was evaluated from the relation

$$\frac{1}{E_r} = \frac{\left(1-\nu_c{}^2\right)}{E_c} + \frac{\left(1-\nu_i{}^2\right)}{E_i} \quad \text{…….....} \qquad (3)$$

where $E_i$ and $\nu_i$, and $E_c$ and $\nu_c$, are the elastic modulus and Poisson's ratio of the indenter and the coating respectively.
The loading curve is an elastic-plastic deformation of the coating and follows equation (4)

$$P = \alpha . h^m \ldots\ldots\ldots\ldots\ldots\ldots\ldots\ldots (4)$$

The constant α and exponent m describes the mechanical properties of the material and geometry of the indenter [1].

The unloading curve also shows elastic and plastic behaviour, and is characterised by equation (5)

$$P = A . \left(h - h_f\right)^n \ldots\ldots\ldots\ldots\ldots (5)$$

The exponent A and n are material constants and are found to take values of 1.3 – 1.5 for a Berkovich indenter, and 2 for a Vickers indenter [1].

From the essential parameters for the hardness evaluation in Fig. 1, the contact depth $h_c$ is the difference between $h_s$ which is the deflection depth of the surface and the maximum depth

$$h_c = h_{max} - h_s \ldots\ldots\ldots\ldots (6)$$

The deflection depth of the surface $h_s$is given in equation (7)

$$h_s = \epsilon . \frac{P_{max}}{S} \ldots\ldots\ldots\ldots\ldots (7)$$

$\epsilon$ is the intercept correction factorand implies the geometry of the tip. For $\epsilon$ = 0.72 the tip will be conic, $\epsilon$ = 0.75 it will bespherical, and for $\epsilon$ = 1, a flat punch. A value of $\epsilon$ = 0.75 best describe the unloadingprocess [1].

The ratio H/E called plasticity index, is widely quoted as a valuable measure in determining the limit of elastic behaviour in a surface contact. It is important in tribology as a characteristic of materials wear. A high plasticity index is often a reliable indicator of a good wear resistance of coatings [2].

## 2.0 Fracture Toughness

Fracture toughness is a property which describes the ability of a material containing a crack to resist fracture, and is one of

the most important properties of any material for virtually all design applications. It is denoted by $K_{IC}$(or simply Kc) and has the units of Pa-$m^{1/2}$.The subscript $_{IC}$ denotes mode I crack opening under a normal tensile stress perpendicular to the crack, since the material can be made deep enough to stand shear (mode II) or tear (mode III).Fracture toughness is a quantitative way of expressing a material's resistance to brittle fracture when a crack is present. If a material has high fracture toughness it will probably undergo ductile fracture. Brittle fracture is very characteristic of materials with less fracture toughness. One critical implications of fracture toughness is that it leads to erosive wear and vice versa.

If the impact of an erosive particle leads to brittle fracture, material is removed from the surface by nucleation and intersection of cracks. In this case, the most relevant material property which determines the erosion resistance is fracture toughness (*Kc*), with hardness (*H*) being a much less significant parameter. When a load is applied such that the value $K_{IC}$ is reached, the crack is in equilibrium and by exceeding it, the crack would rapidly propagate. The use of thin film coatings on hard and flexible substrates is prone to scratches and or fracture during handling which will eventually impact on the suitability of the coatings for many applications. It is therefore important to know this threshold to avoid failure in practice.

Various models have been employed in the determination of the fracture toughness as proposed by different authors. These include among others [3];

$$K_c = 0.0089\left(\frac{E}{H}\right)^{2/5}\frac{P}{al^{1/2}} \quad \text{for} \quad \cong 0.25 \le 1/a \le \cong 2.5 \qquad \text{..... (8)}$$

$$K_c = 0.0122\left(\frac{E}{H}\right)^{2/5}\frac{P}{al^{1/2}} \qquad \text{..... (9)}$$

$$K_c = 0.0319\frac{P}{al^{1/2}} \qquad \text{..... (10)}$$

$$K_c = 0.0143\left(\frac{E}{H}\right)^{2/3}\left(\frac{a}{l}\right)^{1/2}\frac{P}{c^{3/2}} \qquad \text{.....(11)}$$

with c = a + 1

where *E* is the Young modulus, *H* the hardness, *P* the applied load, *a* the half diagonal of the indent and *l* thecrack length.

Fracture toughness of a bulk brittle material can also be calculated within 40% accuracy based on the maximum indentation depth, $P_{max}$ and the crack length, *c*

$$K_C = \alpha\left(\frac{E}{H}\right)^{1/2}\left(\frac{P_{max}}{c^{3/2}}\right) \qquad \text{.....(12)}$$

where P is the applied load, H is the hardness of the thin film, E the elastic modulus determined by nanoindentation, and c is the crack length. The constant α is an empirical constant which depends on the geometry of the indenter, and is 0.0319 for a cube corner indenter geometry[4], and 0.016 ± 0.004 for a Vickers hardness tip [1].

An additional method utilized for measuring fracture toughness involves a lateral scratch, which causes a tangential stress at the trailing edge of the scribe [4].

$$K_C = 2\sigma_{\theta\theta}\left(\frac{c}{\pi}\right)^{1/2}\cdot\sin^{-1}\left(\frac{a}{c}\right) \qquad \text{.....(13)}$$

where *a* is the contact radius and *c* is the half crack. Since *a*/*c* is almost always less than 1/2, sin-1(*x*) ≈ *x* and with $\sigma_{\theta\theta} = P_{max}/\pi a^2$, and equation reduces to:

$$K_C \approx \frac{2P_{max}}{\pi^{3/2}}\cdot\frac{1}{ac^{1/2}} \approx \text{const}\cdot\left(\frac{P_{max}}{c^{3/2}}\right) \qquad \text{.....(14)}$$

The fracture toughness measured in terms of the critical energy-release rate $G_c$ can also be expressed as [5]

$$G_c = \frac{12P_c^2a^2}{t^2l^3\overline{E}}\left[3.467 + 2.315\left(\frac{l}{a}\right)\right]^2 \qquad \text{.....(15)}$$

where $P_c$ is the critical load, $\overline{E}$ is the plane strain tensile modulus defined by $E/(1 - v^2)$, ($E$ =Young's modulus, v = Poisson's ratio), $a$ is the crack length, $t$ is the specimen thickness, and $l$ is the specimen half height, respectively.
The fracture toughness can also be determined using Vickers indentations in which the Vickers diagonals and crack lengths are measured at various loads. The crack length can be determined from [6];

$$c = \frac{(2d_{||} + 2d_{\perp})}{4} + \frac{(a_l + a_r)}{2} \quad \ldots\ldots\ldots\ldots\ldots (16)$$

where $2d_{||}$ and $2d_{\perp}$ are the parallel and perpendicular Vickers diagonals to the coating surface, and $a_l$ and $a_r$ are the left and right crack lengths, respectively.
Using the indentationload, $P$, and total crack length, $c$, the fracture toughness $K$c is determined using the relation [6];

$$K_c = 0.0711(H_v d^{1/2})\left[\frac{E}{H_v}\right]^{2/5}\left[\frac{c}{d}\right]^{-3/2} \quad \ldots\ldots\ldots\ldots\ldots\ldots (17)$$

where $H_v$ and $E$ are the Vickers hardness and elastic modulus, respectively.
This equation is only valid for a 'Half-Penny' crack regime, which occurs when $c/d \geq 02.5$, where $d$ is the Vickers half-diagonal.

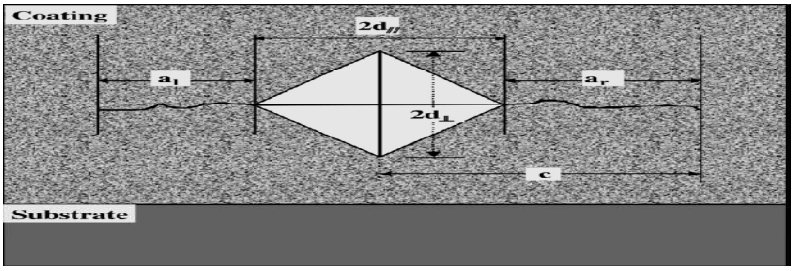


**Fig. 2:** Schematic of the Vickers indentation and crack geometry [6]
There are currently few reports in the literature on the mechanical properties of copper oxides. It hoped this work will add to an understanding of these properties.

## 3.0 Experimental Investigation

The film deposition was performed with a cryo-pumped vacuum chamber (CVC) rf magnetron sputtering unit AST304. The deposition chamber is 25" in diameter with a target-substrate separation of 9.5cm. The materials are solid copper target of 99.99% purity, 8.0" diameter and 6.0mm thick Prior to deposition, the chamber was evacuated to a base pressure of $10^{-6}$ T. Glass slides, silica and silicon wafer which were cleaned ultrasonically with iso-propanol and then washed with de-ionised water were used as substrates. High purity argon and oxygen were used as the sputtering and reactive gases respectively. The target was pre-sputtered in pure Argon atmosphere for 3 minutes to remove oxide layers if any on the surface of the target. All depositions are for duration of five (5) minutes. The deposition conditions are given in Table 1.

**Table 1:** Film deposition condition

| Power (W) | Power density (W/cm2) | Pressure (mT) | Oxygen flow range (sccm) |
|---|---|---|---|
| 200 | 0.6 | 2.0 – 6.0 | 1 – 4 |
| 300 | 0.9 | 2.0 – 6.0 | 1 – 4 |
| 400 | 1.2 | 2.0 – 6.0 | 2 – 6 |
| 500 | 1.5 | 2.0 – 6.0 | 2 – 6 |
| 600 | 1.9 | 2.0 – 6.0 | 2 – 6 |

## 4.0 Film Characterisation

SEM measurement was performed with a Hitachi S-4100 model. AFM imaging was performed on a Digital Instruments Veeco Metrology system. XRD patterns of the prepared films were recorded on a Siemens D5000 X-Ray Diffractometer, using $CuK_\alpha$ radiation to identify the oxide phases present. The crystal planes were identified with the powder cell software. The film thicknesses are evaluated from Optical transmission measurements conducted on nkd Aquila spectrophotometer. Nanoindentation was performed on a Hysitron Tribo-Scope Nanomechanical testing system to obtain Force-Displacement curves for the samples prepared on microscope glass substrates at various loads. The system is incorporated with a 3 plate capacitive transducer attached to a scanning probe microscope. The transducer generates the testing load force and simultaneously measures the applied force and the resulting displacement of the indenter tip. The indenter was calibrated

with a fused quartz sample with a standard reduced modulus of 69.6GPa. Micro indentation tests were performed on film coatings prepared at different rf power to determine the fracture toughness. A Shimadzu Micro Hardness tester with a diamond Vickers indenter was used to apply certain loads on the film coatings prepared on microscope glass substrates to force radial cracks whose length were measured for the evaluation of the fracture toughness.

## 5.0 Results and Discussions

**SEM and AFM Results**

The films prepared at different forward power density, oxygen flow rates and deposition pressures have dense columnar structures but with slightly rough surfaces. The surface roughness was seen to increase with increasing power density. The films prepared at 400W-4sccm-6.0mT and 500W-6sccm-4mT deposition conditions were seen to have columnar structure, smooth surfaces but contain some minor defects. The film prepared at 600W-6sccm-6.0mT deposition condition also has a columnar structure but with a rough surface. The cross-sectional view of the scanning electron micrograph of the films prepared at different deposition conditions are shown in Fig.3. Typical Atomic Force Microscopy (AFM) images are shown in Fig. 4 and Fig. 5

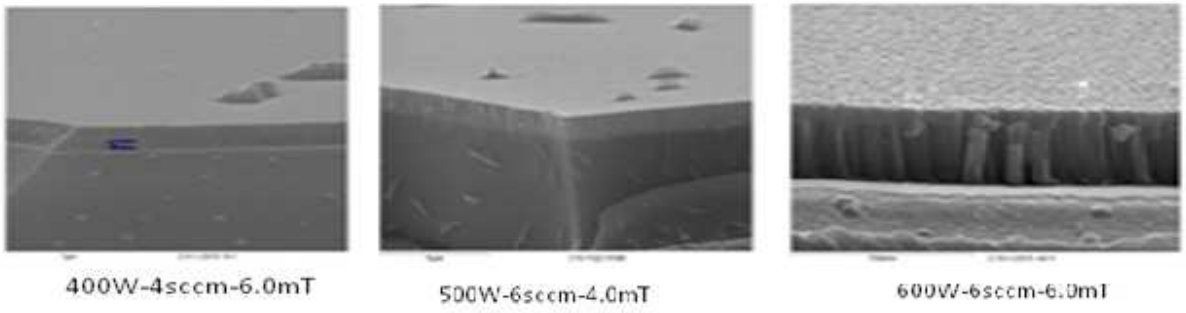


**Fig. 3:** Scanning electron micrograph of films prepared at different deposition conditions

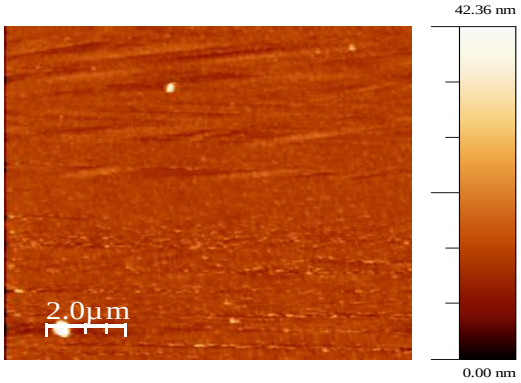


**Fig.4:** AFM topography of film prepared at 300W power, 3sccm oxygen flow and 6.0mT pressure

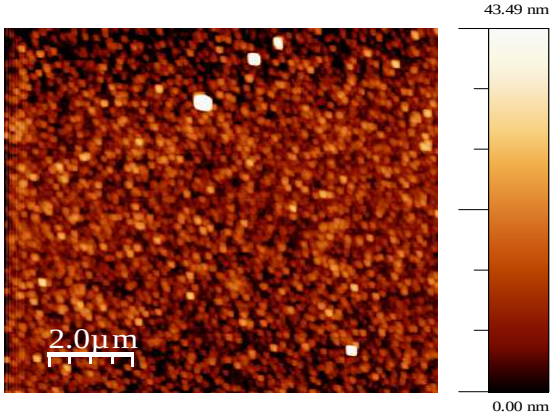


**Fig.5:** AFM topography of film prepared at 500W power, 6sccm oxygen flow and 4.0mT pressure

## 6.0 XRD Results

The X-ray diffraction spectra of the film prepared at 200W-2sccm-6.0mT is polycrystalline with moderate peaks at 2θ = 36.2° (d=2.478Å), and at 2θ = 42.3° (d=2.137Å) corresponding to the (111) and (200) planes of the $Cu_2O$ phase. At 300W-3sccm-6.0mT deposition condition, shows a strong peak at 2θ = 36.5° (d=2.461Å) corresponding to the (111) plane of $Cu_2O$ cubic structure. The film prepared at 400W-4sccm-6.0mT deposition condition depicts a strong peak at 2θ = 36.9° (d= 2.431Å), and a weak peak at 2θ = 42.8° (d= 2.112Å) corresponding to the (111) and (200) planes of the cubic $Cu_2O$ phase. The film prepared at the deposition condition of 500W-6sccm-4.0mT depicts a spectra with strong peak at 2θ = 36.1° (d= 2.488Å) corresponding to the (111) plane of cubic $Cu_2O$ phase, and weak peaks at 2θ = 38.3° (d= 2.350Å), 2θ = 51.8° (d= 1.764Å), and 2θ = 71.3° (d= 1.322Å) which can be attributed to the (111), (112), and ( $\bar{3}12$) planes of the monoclinic CuO phase respectively, and at 2θ = 43.2° (d= 2.093Å) corresponding to the (111) plane of un-oxidised Cu. The film prepared at 600W- 6sccm-6.0mT deposition condition is polycrystalline in nature. The spectra show strong peaks at 2θ = 36.9° (d= 2.434Å) and 2θ = 42.9° (d= 2.102Å) which can be attributed to the (111) and (200) planes of the cubic $Cu_2O$ phase, a medium peak at 2θ = 38.4° (d= 2.344Å) which can be attributed to the (111) plane of the monoclinic CuO phase, and a weak peak at 2θ = 51.6° (d= 1.770Å) which can be attributed to the (112) plane of CuO phase. The X-ray diffraction patterns of films prepared at different deposition conditions are shown in Fig. 6.

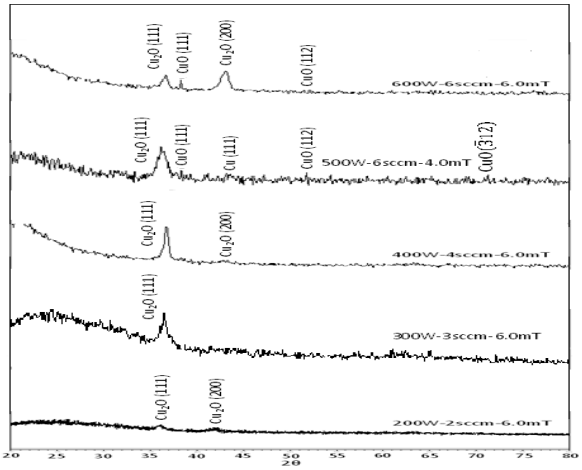


**Fig. 6:** X-ray diffraction pattern of films prepared at different deposition conditions

## 7.0 Fracture Toughness Determination

The hardness and reduced modulus were obtained from Nanoindentation extracted from the load-displacement fitting. Equation (3) was used to evaluate the elastic modulus of the film coatings using the values of 1141GPa and 0.07 [1] as the elastic modulus and Poisson's ratio of the indenter (diamond). The indentation was performed at ten (10) different positions and an average of the reduced modulus and hardness was evaluated for the determination of the elastic modulus of the film coatings and fracture toughness respectively.

Due to the mixed nature of the coatings ($Cu_2O$ + CuO), and in view of their different values of Poisson's ratio of 0.39 [7] and 0.445 [8] for CuO and $Cu_2O$ respectively, an average value of 0.42was used as the Poisson's ratio of the film coatings.The crack lengths resulting from the micro indentation test were measured, although not every load produces the cracks.

Typical micro indentations on the films prepared at 500W powers, 6.0sccm oxygen flow rate and 4.0mT pressure is shown in Fig. 7.

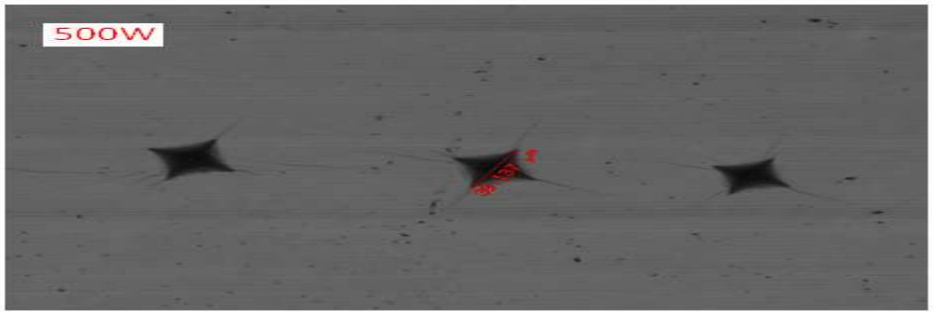


**Fig. 7:** Vickers indentation on a film prepared at 500W on glass substrate

The average hardness determined by Nanoindentation, and the measured crack lengths at different loads were used in equation (12) to evaluate the fracture toughness. There is limited information in the literature on the elastic modulus of copper oxides, in particular copper I oxide. Reports available includes CuO elastic modulus of 70 – 300GPa by Tan et al [9], and 89.6GPa by Wu et al [7]. Firmansyah et al [8] have reported Young's modulus of $3.0x10^{10}$ $Nm^{-2}$ (30 GPa) for $Cu_2O$.
Table 2 shows tabulations of the average hardness, reduced modulus, elastic modulus, plasticity index, and fracture toughness of the films at different loads and deposition conditions.

**Table 2a:** Fracture toughness, average hardness, reduced modulus, elastic modulus, and plasticity index at various loads for film prepared at 600W power

| Sample: C10I231542 | | Load P (N) | Crack Length c (μm) | Fracture Toughness $K_{IC}$ ($MPa.m^{½}$) |
|---|---|---|---|---|
| Power: | 600W | 5.89 | 55.78 | 0.80 ± 0.34 |
| Pressure: | 6.0mT | | | |
| Oxygen flow: | 6.0 sccm | 5.40 | 52.36 | 0.81 ± 0.34 |
| Hardness: | 4.13 GPa | | | |
| Elastic Modulus: | 52.24 GPa | 4.91 | 46.89 | 0.87 ± 0.34 |
| Reduced Modulus: | 60.07 GPa | | | |
| Thickness: | 328.39nm | 3.43 | 31.84 | 1.09 ± 0.34 |
| Major Oxide Phase: | $Cu_2O$+CuO | | | |
| Plasticity index: | 0.079 | | | |

**Table 2b:** Fracture toughness, average hardness, reduced modulus, elastic modulus, and plasticity index at various loads for film prepared at 500W power

| Sample: C10K111131 | | Load P (N) | Crack Length c (μm) | Fracture Toughness $K_{IC}$ ($MPa.m^{½}$) |
|---|---|---|---|---|
| Power: | 500W | 5.89 | 42.85 | 1.36 ± 0.49 |
| Pressure: | 3.0mT | | | |
| Oxygen flow: | 6.0 sccm | 4.91 | 34.69 | 1.55 ± 0.49 |
| Hardness: | 4.22 GPa | | | |
| Elastic Modulus: | 68.74 GPa | 4.41 | 34.17 | 1.43 ± 0.49 |
| Reduced Modulus: | 77.80 GPa | | | |
| Thickness: | 89.58 nm | 3.43 | 31.84 | 1.09 ± 0.49 |
| Major Oxide Phase: | Amorphous | | | |
| Plasticity index | 0.061 | | | |

**Table 2c**: Fracture toughness, average hardness, reduced modulus, elastic modulus, and plasticity index at various loads for film prepared at 400W power

| **Sample: C10I231519** | | Load P (N) | Crack Length c (μm) | Fracture Toughness $K_{IC}$ ($MPa.m^{½}$) |
|---|---|---|---|---|
| Power: | 400W | 4.91 | 56.44 | 0.70 ± 0.32 |
| Pressure: | 4.0mT | | | |
| Oxygen flow: | 6.0 sccm | 4.41 | 44.70 | 0.90 ± 0.32 |
| Hardness: | 4.52 GPa | | | |
| Elastic Modulus: | 65.29 GPa | 3.92 | 40.32 | 0.93 ± 0.32 |
| Reduced Modulus: | 74.15 GPa | | | |
| Thickness: | 192.74 nm | 2.94 | 30.23 | 1.08 ± 0.32 |
| Major Oxide Phase: | $Cu_2O$ | | | |
| Plasticity index | 0.069 | | | |

**Table 2d:** Fracture toughness, average hardness, reduced modulus, elastic modulus, and plasticity index at various loads for film prepared at 300W power

| Sample: C10K301241 | | Load P (N) | Crack Length c (μm) | Fracture Toughness $K_{IC}$ (MPa.m$^{½}$) |
|---|---|---|---|---|
| Power: | 300W | 4.91 | 59.73 | 0.64 ± 0.26 |
| Pressure: | 3.0mT | | | |
| Oxygen flow: | 6.0 sccm | 2.94 | 37.01 | 0.79 ± 0.26 |
| Hardness: | 4.72 GPa | | | |
| Elastic Modulus: | 67.44 GPa | | | |
| Reduced Modulus: | 76.43 GPa | | | |
| Thickness: | 127.41 nm | | | |
| Major Oxide Phase: | $Cu_2O$ | | | |
| Plasticity index | 0.07 | | | |

**Table 2e:** Fracture toughness, average hardness, reduced modulus, elastic modulus, and plasticity index at various loads for film prepared at 200W power

| Sample: C9I221020 | | Load P (N) | Crack Length c (μm) | Fracture Toughness $K_{IC}$ (MPa.m$^{½}$) |
|---|---|---|---|---|
| Power: | 200W | 3.43 | 55.09 | 0.97 ± 0.30 |
| Pressure: | 2.0mT | | | |
| Oxygen flow: | 3.0 sccm | | | |
| Hardness: | 4.99 GPa | | | |
| Elastic Modulus: | 66.69 GPa | | | |
| Reduced Modulus: | 75.63 GPa | | | |
| Thickness: | 73.55 nm | | | |
| Major Oxide Phase: | $Cu_2O$ | | | |
| Plasticity index | 0.075 | | | |

Very long cracks were obtained at comparatively low loads for the films prepared at 300W, 200W, and as shown in Tables 2 (d and e).

The fracture toughness was seen to decrease with increasing load for the cases where cracks were generated by different loads, even though not in a uniform pattern for the films investigated.

The lower values of the fracture toughness are indications that the copper oxide thin film material is characterized by brittle fracture. The literature is lacking on the investigation of fracture toughness and other mechanical properties of copper oxide thin films.

## 8.0 Conclusion

Nanoindentations and Micro indentations are performed at various loads on copper oxide thin films prepared on glass slides at various deposition conditions. The films are found to be predominantly of the cuprous oxide ($Cu_2O$) phase. The mechanical properties evaluated comprises of hardness found to be in the range of 4.13 – 4.99 GPa, elastic modulus of 52.24 – 66.69 GPa, plasticity index of 0.061 – 0.079, and fracture toughness of 0.64 ± 0.26 - 1.55 ± 0.49 MPa.m$^{½}$. The findings are indications that copper oxide thin films exhibit fracture brittle in nature.

## 9.0 References

[1] Thomas Hellwig; Physical, electrochemical, and mechanical characterisation of amorphous boron phosphide by plasma enhanced chemical vapour deposition (PECVD), PhD thesis, University of the West of Scotland, 2009

[2] L. Brabec, P. Bohac, M. Stranyanek, R. Ctvrtlik and M. Kocirik; Microporous and Mesoporous Materials Vol. 94, Issues 1-3, 8 (Sept.2006) p226 – 233

[3] Roman A. A, Chicot D, and Lesage J; Surface and Coatings Technology, 155 (2002) 161- 168

[4] Volinsky A. A, Vella J. B, and Gerberich W. W; Thin Solid Films 429 (2003) 201 –210

[5] Lee H. Y and Jin Yu; Materials Science and Engineering **A**277 (2000) 154 – 160

[6] Lima M. M, Godov C, Modenesi P.J, Avelar-Batista J.C, Davison A, and Mathews A; Surface and Coatings Technology 177 – 178 (2004) 489 – 496

[7] Wu E, Yang A.J.D, and Shao C-A; 2004 Electronic Components and Technology Conference, (0-7803-8365-6/04)L.

[8] Firmansyah D. A, Kim T, Kim S, Sullivan K, Zachariah M. R, and Lee D; Langmuir 2009, 25(12), 7063–7071

[9] Tan E.P.S, Zhu Y, Yu T, Dai L, Sow C.H, Tan V.B.C, and Lim C.T; Applied Physics Letters 90, 163112 (2007)